The NaK $1(b)\,^3\Pi_{\Omega=0}$ state hyperfine structure and the $1(b)\,^3\Pi_{\Omega=0} \sim 2(A)\,^1\Sigma^+$ spin–orbit interaction

P. Burns, A. D. Wilkins, A. P. Hickman, and J. Huennekens
Department of Physics, Lehigh University, 16 Memorial Drive East, Bethlehem, Pennsylvania 18015

(Received 30 August 2004; accepted 9 November 2004; published online 7 February 2005)

We have measured the hyperfine structure of mutually perturbing rovibrational levels of the $1(b)\,^3\Pi_0$ and $2(A)\,^1\Sigma^+$ states of the NaK molecule, using the perturbation-facilitated optical-optical double resonance method with copropagating lasers. The unperturbed $1(b)\,^3\Pi_0$ levels are split into four hyperfine components by the Fermi contact interaction $b_F\mathbf{I}\cdot\mathbf{S}$. Mixing between the $1(b)\,^3\Pi_0$ and $2(A)\,^1\Sigma^+$ levels imparts hyperfine structure to the nominally singlet component of the perturbed levels and reduces the hyperfine splitting of the nominally triplet component. Theoretical analysis relates these observations to the hyperfine splitting that each $1(b)\,^3\Pi_0$ level would have if it were not perturbed by a $2(A)\,^1\Sigma^+$ level. Using this analysis, we demonstrate that significant hyperfine splitting arises because the $1(b)\,^3\Pi_0$ state cannot be described as pure Hund's case (a). We determine b_F for the $1(b)\,^3\Pi_0$ levels and also a more accurate value for the magnitude of the singlet-triplet spin–orbit coupling $H_{SO}=\langle 1(b)\,^3\Pi_0(v_b,J)|\mathbf{H}_{SO}|2(A)\,^1\Sigma^+(v_A,J)\rangle$. Using the known spectroscopic constants of the $1(b)\,^3\Pi$ state, we obtain $b_F=0.009\,89\pm0.000\,27\ \mathrm{cm}^{-1}$. The values of $|H_{SO}|$ are found to be between 2 and 3 cm^{-1}, depending on v_b, v_A, and J. Dividing $|H_{SO}|$ by calculated vibrational overlap integrals, and taking account of the $1(b)\,^3\Pi_\Omega$ rotational mixing, we can determine the magnitude of the electronic part H_{el} of H_{SO}. Our results yield $|H_{el}|=(16.33\pm0.15)\ \mathrm{cm}^{-1}$, consistent with our previous determinations using different techniques.
 [DOI: 10.1063/1.1844293]

I. INTRODUCTION

Mixed $b\,^3\Pi_0 \sim A\,^1\Sigma^+$ window levels have been used to study a large number of alkali triplet states using the "perturbation-facilitated optical-optical double resonance" (PFOODR) technique.[1–14] In addition, considerable effort has been focused on the details of the individual $A\,^1\Sigma^+$ and $b\,^3\Pi$ states and the spin–orbit coupling between them.[8,15–30] This interest reflects the importance of these states in many applications. For example, understanding the $b\,^3\Pi_0 \sim A\,^1\Sigma^+$ perturbations is important for ultracold atom studies where fine structure changing collisions occurring through these perturbations can result in trap loss.[31,32] The present work explores the hyperfine structure of mutually perturbing, rovibrational levels of the NaK $1(b)\,^3\Pi_0$ and $2(A)\,^1\Sigma^+$ states.

Most studies of the $b\,^3\Pi_0 \sim A\,^1\Sigma^+$ spin–orbit perturbations have focused on the homonuclear molecules Li_2,[15] Na_2,[16,17,21–23,25] and K_2,[19,28] although in recent years similar studies on the heteronuclear molecules NaK,[24] NaRb,[29] and RbCs (Ref. 30) have also been undertaken. Techniques including examination of anomalous lifetimes[33,34] or transition intensities,[15] and deperturbation of high-resolution spectra of perturbed levels[16,19,21,23] have been employed to analyze these interactions. Previously in our lab,[24] we determined values for the NaK $1(b)\,^3\Pi_0 \sim 2(A)\,^1\Sigma^+$ spin–orbit interaction matrix elements using high-resolution measurements of pairs of perturbed level energies in combination with the deperturbed $1(b)\,^3\Pi_0$ molecular constants of Ross *et al.*[18] These values were in good agreement with less accurate intensity measurements also carried out as part of that work.[24]

Investigations of the hyperfine structure of the $b\,^3\Pi$ state have also focused primarily on the homonuclear molecules.[3–6,8–10,12,21,35,36] However, many PFOODR studies address heteronuclear as well as homonuclear molecules, so it is equally important to understand the $b\,^3\Pi_0$ hyperfine structure of the heteronuclear molecules. In fact, there are interesting issues regarding the hyperfine structure of the NaK $1(b)\,^3\Pi$ state. Previous investigators have studied the hyperfine structure of high v ($\sim$62), low J, rovibrational levels perturbed by nearby $1(B)\,^1\Pi$ and $2(c)\,^3\Sigma^+$ levels.[37,38] Ishikawa *et al.*[37] observed measurable hyperfine splittings in the $1(b)\,^3\Pi_0$ state only for levels that are strongly perturbed by $2(c)\,^3\Sigma^+$ levels. The ratio $A_v/(B_vJ) \sim 173/J$ (where A_v is the spin–orbit interaction constant and B_v is the rotational constant) indicates that for typical values of J (20–50), the NaK $1(b)\,^3\Pi$ state should lie intermediate between the Hund's case (a) and case (b) coupling schemes, but closer to case (a). In the pure Hund's case (a) limit, the analysis of Frosch and Foley[39] indicates that a $^3\Pi_0$ state should exhibit negligible magnetic dipole hyperfine structure. In alkali molecules, the dominant contribution to the hyperfine structure is the magnetic dipole Fermi contact interaction $b_F\mathbf{I}\cdot\mathbf{S}$.[37,40–42] Therefore, any observed hyperfine structure in $1(b)\,^3\Pi_0$ levels must be attributed to interactions involving the $1(b)\,^3\Pi_1$ and $1(b)\,^3\Pi_2$ levels.[38] Earlier work in our lab on the $1\,^3\Delta$ state of NaK (Ref. 11) using the PFOODR technique with copropagating and counterpropagating beams suggested that the hyperfine structure of the $1(b)\,^3\Pi_0$ state was not negligible. Our

present work clearly demonstrates that the NaK $1(b)\,^3\Pi_0$ state cannot be described as pure case (a) and does indeed display significant hyperfine splittings.

In the present work we have measured the hyperfine splittings of selected NaK $1(b)\,^3\Pi_0(v_b,J)\sim 2(A)\,^1\Sigma^+(v_A,J)$ mixed levels using a variation of the PFOODR technique with copropagating lasers. These mixed levels display hyperfine structure in proportion to the amount of $1(b)\,^3\Pi_0$ character they possess. By sweeping through states with different values of the quantum number J, we are able to monitor the changes in the hyperfine structure for different amounts of singlet-triplet mixing. We observe a reduction in the hyperfine splittings of the nominally "triplet" levels and a corresponding increase in the splitting of the nominally "singlet" levels as the value of J approaches that of the most strongly interacting levels. We have developed a model that permits a direct determination of the spin–orbit coupling matrix elements and the mixing coefficients from the measured hyperfine structure of a pair of perturbed rovibrational levels. Further analysis enables us to determine the value of the Fermi contact constant b_F for the $1(b)\,^3\Pi_0$ state.

This paper is organized as follows: Section II describes the experimental setup and an analysis of the expected line splittings in the copropagating and counterpropagating geometries. Section III A discusses the expected hyperfine splittings of a $^3\Pi_0$ state, including effects that arise when the state is not pure case (a). Section III B presents an analysis of the hyperfine structure of mixed singlet-triplet levels. These theoretical results permit the Fermi contact constant and the $1(b)\,^3\Pi_0\sim 2(A)\,^1\Sigma^+$ spin–orbit matrix elements to be determined from the measured line positions and hyperfine splittings. The principal experimental results of this work are presented in Sec. IV, and a few concluding remarks can be found in Sec. V.

II. EXPERIMENT

A. Setup

The experimental setup is the same as used in our previous PFOODR studies of NaK and is shown in Fig. 1 of Ref. 11. Briefly, sodium and potassium metals are placed within a crossed four-arm heat pipe oven.[43] When the center of the oven is heated, a vapor of NaK, Na_2, and K_2 molecules, as well as sodium and potassium atoms, is produced. Selected levels of the NaK $1(b)\,^3\Pi_0\sim 2(A)\,^1\Sigma^+$ manifold are excited from the $1(X)\,^1\Sigma^+$ ground state using a Coherent model 699-29 cw dye laser operating in the 710–770 nm range with LD 700 dye. A Coherent model 899-29 Ti:sapphire laser operating in the 730–920 nm range is then used to probe these levels on transitions to higher lying states. In some cases, the roles of the dye and Ti:sapphire lasers are reversed. The dye laser power is 150–400 mW while the Ti:sapphire power is in the range 300–700 mW. Both lasers have linewidths of ~500 kHz. Absorption of pump and probe laser photons is monitored by detecting fluorescence emerging from the side arms of the heat pipe using two different detectors. A freestanding Hamamatsu R406 photomultiplier tube, with a 700–1000 nm bandpass filter mounted in front of it, detects total $2(A)\,^1\Sigma^+ \rightarrow 1(X)\,^1\Sigma^+$ red and near-IR fluorescence, which allows us to set the pump laser to a particular $1(b)\,^3\Pi_0(v_b,J)\sim 2(A)\,^1\Sigma^+(v_A,J)\leftarrow 1(X)\,^1\Sigma^+(v_X,J\pm 1)$ transition (either the mostly singlet or the mostly triplet component of the upper state). The pump laser is chopped and the output of the photomultiplier tube (PMT) is sent to a lock-in amplifier. A freestanding Hamamatsu 928 PMT, equipped with green or violet bandpass filters, monitors the total green $^3\Lambda\rightarrow 1(a)\,^3\Sigma^+$ or total violet $^1\Lambda\rightarrow 1(X)\,^1\Sigma^+$ fluorescence from higher lying triplet and singlet states, respectively, that are populated by Ti:sapphire (probe) laser photons as the laser frequency is scanned. The pump laser wavemeter is calibrated by comparing frequencies of I_2 laser-induced fluorescence lines to those listed in the iodine atlas.[44] The probe laser wavemeter is calibrated using optogalvanic signals from neon transitions in a hollow cathode lamp. Absolute energies of $2(A)\,^1\Sigma^+$ and $1(b)\,^3\Pi_0$ levels studied here are considered to be accurate to within 0.01 cm^{-1}. However, splittings between individual hyperfine components are determined to much higher accuracy, typically 0.001 cm^{-1} (30 MHz).

B. Hyperfine structure in the copropagating and counterpropagating geometries

In the experimental setup, the pump and the probe laser beams can be counterpropagated or copropagated along the axis of the heat pipe oven. In previous studies of the hyperfine structure of high-lying triplet states,[5,6,9–11,13] the counterpropagating pump/probe geometry was used because, in that configuration, the hyperfine structure of the intermediate state cancels for the most part.[11] However, direct measurements of the hyperfine structure of individual $1(b)\,^3\Pi$ state rovibrational levels are possible using PFOODR spectroscopy in a copropagating geometry. To understand how this works, we refer to Eq. (9) of Ref. 11, which gives the $^{1,3}\Lambda(v_\Lambda,J\pm 1)\leftarrow 1(b)\,^3\Pi_\Omega(v_b,J)\leftarrow 1(X)\,^1\Sigma^+(v_X,J\pm 1)$ OODR pump/probe laser resonance condition. In Ref. 11, the upper state considered was the $1\,^3\Delta$ state. However, because the $1(b)\,^3\Pi_\Omega(v_b,J_b)$ levels we consider are actually singlet/triplet mixtures (usually $\Omega=0$), the upper state $^{1,3}\Lambda(v_\Lambda,J_\Lambda)$ can, in fact, be either a singlet or a triplet. In Ref. 11, it is shown that the observed splittings of the OODR transition are determined by the upper state level hyperfine structure, minus $[1\mp(\omega_{\text{probe}}/\omega_{\text{pump}})]$ times the hyperfine splitting of the intermediate $1(b)\,^3\Pi_\Omega(v_b,J_b)$ level [where the upper (minus) sign corresponds to the case of counterpropagating pump and probe lasers, and the lower (plus) sign is used for copropagating lasers]. Note that Eq. (9) of Ref. 11 was obtained using the assumption that the hyperfine structure of the ground state $1(X)\,^1\Sigma^+$ is negligible.

Since ω_{probe} and ω_{pump} are approximately equal, the hyperfine structure of the intermediate $1(b)\,^3\Pi_\Omega$ level contributes little to the observed structure of the probe transition in the counterpropagating geometry. Thus this geometry is ideal for studying the hyperfine structure of the upper state. However, for the copropagating case, the hyperfine splitting of the $1(b)\,^3\Pi_\Omega$ level will contribute to the observed line splittings with almost twice its actual value. Thus the copropagating geometry can be used to study the hyperfine structure of any

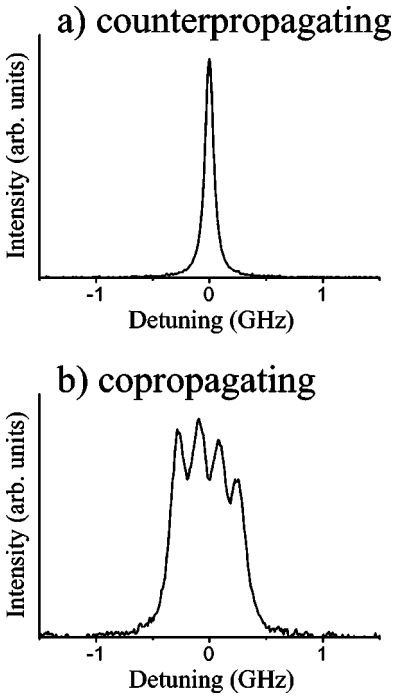

FIG. 1. Hyperfine structure of the $3\,^1\Pi(v=13,J=46)\leftarrow 1(b)\,^3\Pi_{\Omega=0}(v=18,J=45)\leftarrow 1(X)\,^1\Sigma^+(v=0,J=46)$ pump/probe transition using (a) the counterpropagating geometry and (b) the copropagating geometry.

$1(b)\,^3\Pi_\Omega$ level with sufficient singlet amplitude that it can be directly excited from the singlet ground state. If we choose an upper state that has negligible hyperfine structure, then the probe laser transition line shapes will provide a direct measurement of the $1(b)\,^3\Pi_\Omega(v_b,J_b)$ hyperfine structure.

Note that Eq. (9) of Ref. 11 was based on the assumption that the pump laser frequency was held fixed to line center of the $1(b)\,^3\Pi_\Omega(v_b,J_b)\leftarrow 1(X)\,^1\Sigma^+(v_X,J_b\pm 1)$ transition while the probe laser frequency was scanned. However, a similar analysis applies to the case where the probe frequency is fixed and the pump frequency is scanned. Both techniques were used in the present work, depending on the various transition frequencies, in order to take advantage of the superior scanning operation of the Ti:sapphire laser.

The dominant $b_F\mathbf{I}\cdot\mathbf{S}$ Fermi contact contribution to the hyperfine splitting is zero for spin-singlet states. Therefore we carry out a singlet$\leftarrow$triplet$\leftarrow$singlet PFOODR experiment in the copropagating geometry in order to observe the hyperfine splitting of the intermediate $1(b)\,^3\Pi_0(v_b,J_b)$ level without contamination from the upper state hyperfine structure. Figures 1(a) and 1(b) display $3\,^1\Pi(v=13,J=46)\leftarrow 1(b)\,^3\Pi_0(v=18,J=45)\leftarrow 1(X)\,^1\Sigma^+(v=0,J=46)$ PFOODR signals recorded using the counterpropagating and copropagating geometries, respectively. The former shows that indeed the $3\,^1\Pi$ state has no observable hyperfine splitting, while the latter shows the $1(b)\,^3\Pi_0(v=18,J=45)$ level hyperfine splittings (multiplied by the factor $[1+(\omega_{\text{probe}}/\omega_{\text{pump}})]$). If the intermediate state is a $1(b)\,^3\Pi_0(v_b,J)\sim 2(A)\,^1\Sigma^+(v_A,J)$ mixed level (which is required in order for the singlet$\leftrightarrow$triplet transitions to be observable), the observed hyperfine structure of the probe transition line shape will reflect the triplet amplitude of that mixed level.

III. THEORETICAL ANALYSIS

A. Hyperfine structure of the NaK $1(b)\,^3\Pi_0$ state

We base our analysis on the following model Hamiltonian:[45–49]

$$\mathbf{H}=\mathbf{H}_{\text{rot}}+A\mathbf{L}\cdot\mathbf{S}+b_F\mathbf{I}\cdot\mathbf{S} \tag{1}$$

where $\mathbf{H}_{\text{rot}}$ is the rotational Hamiltonian, $A\mathbf{L}\cdot\mathbf{S}$ is the spin–orbit interaction, and $b_F\mathbf{I}\cdot\mathbf{S}$ is the Fermi contact interaction.[40] We have dropped certain small hyperfine terms to arrive at Eq. (1); details about these terms are found in our previous work[11] and in the original treatments.[39,40] As usual, $\mathbf{L}$ is the electron orbital angular momentum, $\mathbf{S}$ is the total electron spin, and $\mathbf{I}$ is the nuclear spin. We take $\mathbf{I}$ to be the nuclear spin of Na only ($I=3/2$). Previous work[50] as well as our own calculations[51] support this approximation. The nuclear magnetic moment of Na is much larger than that of K, and for the molecular orbitals of the $1(b)\,^3\Pi_0$ state, the electron spin density is also larger at the Na nucleus than at the K nucleus.

The present situation is similar to the case we analyzed in Ref. 13, so we summarize our methodology very briefly. We calculate energies by finding the eigenvalues of the model Hamiltonian Eq. (1), using appropriate values of the coupling constants. For each value of the total angular momentum quantum number F, we diagonalize a 12×12 matrix representation of $\mathbf{H}$, using a set of basis functions $|\alpha NSJI;FM_F\rangle$. For these functions, α denotes the electronic state and vibrational level, and the quantum numbers correspond to the coupling $\mathbf{N}+\mathbf{S}=\mathbf{J}$, and $\mathbf{J}+\mathbf{I}=\mathbf{F}$, where $\mathbf{N}$ is the total angular momentum apart from spin. In the present work, the parameters in the Hamiltonian, Eq. (1), will lead to a coupling scheme intermediate between Hund's case ($b_{\beta J}$) and Hund's case (a_β), but the case ($b_{\beta J}$) basis functions can still be used.

We expect that each $1(b)\,^3\Pi_0$ level will be split into four closely spaced states by the hyperfine interaction term. If the original level has quantum numbers v and J, the model Hamiltonian [Eq. (1)] leads to the states

$$|1(b)\,^3\Pi_0(v)JI;FM_F\rangle,\quad F=J-\tfrac{3}{2},\ J-\tfrac{1}{2},\ J+\tfrac{1}{2},\ J+\tfrac{3}{2}. \tag{2}$$

For the large values of F that we consider, and in the absence of interactions with other electronic states, the splitting between any two adjacent levels within the four states defined by Eq. (2) will be about the same, and we denote the average splitting of these triplet states by ΔE^0_{hfs}. The energies of the four states must be calculated by separate matrix diagonalizations for each value of F.

We have used our model to look for a relation between the Fermi hyperfine coupling constant b_F in Eq. (1) and the observed splitting ΔE^0_{hfs} of the $1(b)\,^3\Pi_0$ state. We performed calculations for many different values of the coupling constants, and we probed in particular the ratio of the observed splitting ΔE^0_{hfs} to the coupling constant b_F, for small values of b_F. By examining the calculated ratio $\Delta E^0_{\text{hfs}}/b_F$ for different values of A, B, and J, we found that to a very good approximation for large J,

$$\frac{\Delta E^0_{\rm hfs}}{b_{\rm F}} = \frac{\chi}{\sqrt{1+\chi^2}}, \tag{3}$$

where χ is a dimensionless parameter that determines where the coupling scheme lies on the continuum between Hund's case (a) and Hund's case (b):

$$\chi = \frac{2B\left(J+\frac{1}{2}\right)}{\Lambda A}. \tag{4}$$

The limit $\chi=0$ corresponds to pure case (a), and in that limit Eq. (3) reduces to the established result[39,40] that the magnetic dipole hyperfine splitting $\Delta E^0_{\rm hfs}$ of a $^3\Pi_0$ state is zero in pure case (a). However, the NaK $1(b)\,^3\Pi_0$ state is not pure case (a), and our results indicate that the levels will exhibit a splitting proportional to $b_{\rm F}$. We emphasize that Eq. (3) is based on the limit $b_{\rm F}\to 0$. In practice, this condition means that the hyperfine splitting should be smaller than the fine structure splitting (governed by A) and smaller than the rotational splitting (governed by B). Plots of $\Delta E^0_{\rm hfs}/b_{\rm F}$ versus χ for different values of A, B, and J suggest that the proposed functional dependence on χ describes the essential features of the observed small hyperfine splittings.

We regard Eq. (3) as an approximate relation that facilitates estimates of A or $b_{\rm F}$ directly from the measured data. If the conditions assumed for its validity are not fulfilled, a more elaborate fitting program should be used to find the values that best fit the data.

B. Spin–orbit matrix element and mixing coefficients

We now consider additional effects that arise because the rovibrational levels of the $1(b)\,^3\Pi_0$ state are coupled with those of the $2(A)\,^1\Sigma^+$ state by the spin–orbit Hamiltonian. This spin–orbit coupling is an additional effect not included in the term $A\mathbf{L}\cdot\mathbf{S}$ in the model Hamiltonian [Eq. (1)], which only couples states of the same total spin quantum number S. The term we now consider is given by

$$H_{\rm SO} = \langle 1(b)\,^3\Pi_0(v_b)JI;FM_F|\mathbf{H}_{\rm SO}|2(A)\,^1\Sigma^+(v_A)JI;FM_F\rangle. \tag{5}$$

As a result of $H_{\rm SO}$, rovibrational levels belonging to the $2(A)\,^1\Sigma^+$ and the $1(b)\,^3\Pi_0$ states may couple and form mixed singlet-triplet levels. Closely spaced pairs of levels of these two electronic states with the same quantum numbers J and F can be expressed as linear combinations of unperturbed states:

$$|\Psi_L\rangle = \cos\theta|2(A)\,^1\Sigma^+(v_A)JI;FM_F\rangle - \sin\theta|1(b)^3\Pi_0(v_b)JI;FM_F\rangle, \tag{6}$$

$$|\Psi_U\rangle = \sin\theta|2(A)^1\Sigma^+(v_A)JI;FM_F\rangle + \cos\theta|1(b)^3\Pi_0(v_b)JI;FM_F\rangle, \tag{7}$$

where the subscripts L and U designate the lower and upper states of the pair, respectively. The effect of this mixing is that both $|\Psi_L\rangle$ and $|\Psi_U\rangle$ will exhibit hyperfine splitting proportional to the amount of their triplet character. Thus we can estimate the magnitude of $H_{\rm SO}$ from the observed hyperfine splittings of the perturbed window levels.

We analyze the hyperfine splittings by considering four independent two-state models. Neglecting $H_{\rm SO}$, the $2(A)\,^1\Sigma^+$ rovibrational level has four degenerate hyperfine levels, all with energy E^0_Σ, and the $1(b)\,^3\Pi_0$ rovibrational level has four distinct hyperfine levels denoted $E^0_{\Pi1},\ldots,E^0_{\Pi4}$. When $H_{\rm SO}$ is "turned on," pairs of levels with the same F are pushed apart by the interaction. The lower mixed state is now split into four levels $L_1,\ldots,L_4$, and the upper mixed state is split into levels $U_1,\ldots,U_4$. According to Eq. (2) and the text thereafter, each pair of states (L_i,U_i) has a different value of F. If we neglect the interactions with other more distant rovibrational levels and assume that $H_{\rm SO}$ is independent of F, we can write the energies of each pair (L_i,U_i) using two-state formulas:

$$U_i = \tfrac{1}{2}(E^0_{\Pi i}+E^0_\Sigma) + \tfrac{1}{2}\sqrt{(E^0_{\Pi i}-E^0_\Sigma)^2+4|H_{\rm SO}|^2}, \tag{8}$$

$$L_i = \tfrac{1}{2}(E^0_{\Pi i}+E^0_\Sigma) - \tfrac{1}{2}\sqrt{(E^0_{\Pi i}-E^0_\Sigma)^2+4|H_{\rm SO}|^2}. \tag{9}$$

For a given pair of adjacent levels (U_i,U_{i+1}) and (L_i,L_{i+1}), we can solve four equations [Eqs. (8) and (9) for i, $i+1$] for the unknown unperturbed levels E^0_Σ, $E^0_{\Pi i}$, $E^0_{\Pi i+1}$, and the coupling parameter $|H_{\rm SO}|$ in terms of the measured energies U_i, U_{i+1}, L_i, and L_{i+1} (see Ref. 52 for details). The solution is

$$|H_{\rm SO}|^2 = \frac{\Delta U\Delta L\left[(U-L)^2-\frac{1}{4}(\Delta U+\Delta L)^2\right]}{(\Delta U+\Delta L)^2} \approx \frac{\Delta U\Delta L(U-L)^2}{(\Delta U+\Delta L)^2}, \tag{10}$$

where we have introduced the notation $\Delta U\equiv U_{i+1}-U_i$, $\Delta L\equiv L_{i+1}-L_i$, $U\equiv\frac{1}{2}(U_i+U_{i+1})$, and $L\equiv\frac{1}{2}(L_i+L_{i+1})$, and where in the last step we have used the fact that the splittings of the upper and lower levels are generally very much smaller than the differences between the levels; ΔU, $\Delta L\ll(U-L)$. The unperturbed $2(A)\,^1\Sigma^+$ level energy is given by[52]

$$E^0_\Sigma = \frac{U\Delta L+L\Delta U}{\Delta U+\Delta L}, \tag{11}$$

and the average energy of the unperturbed $1(b)^3\Pi_0$ levels is

$$E^0_\Pi \equiv \frac{1}{2}(E^0_{\Pi i}+E^0_{\Pi i+1}) = \frac{U\Delta U+L\Delta L}{\Delta U+\Delta L}. \tag{12}$$

It is also straightforward to demonstrate[52] that

$$\Delta E^0_{\rm hfs} \equiv E^0_{\Pi i+1}-E^0_{\Pi i} = \Delta U+\Delta L, \tag{13}$$

which shows that the original splitting of the unperturbed $1(b)^3\Pi_0$ level is exactly equal to the sum of the splittings of the upper and lower mixed levels.

Finally, the mixing angle θ defined in Eqs. (6) and (7) can be obtained by finding the eigenvectors of the appropriate two-state Hamiltonian. In principle, a different value would be obtained for each (L_i,U_i) pair. However, for all levels studied in the present work, ΔU, $\Delta L\ll(U-L)$ holds to an excellent approximation, and we expect that each (L_i,U_i) pair will have essentially the same mixing angle. Thus we find[52]

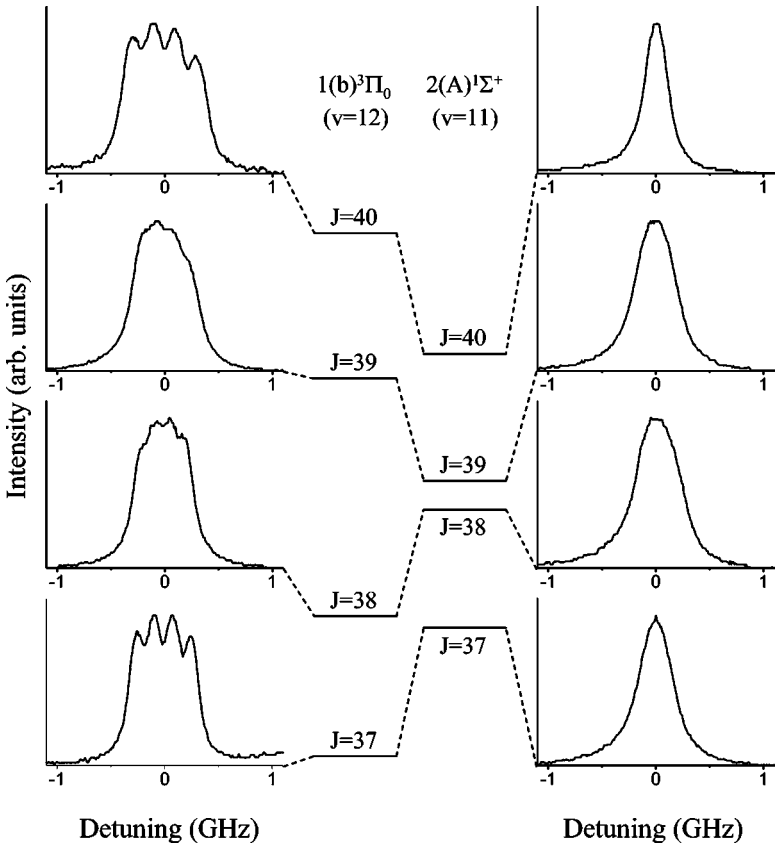

FIG. 2. Double resonance line shapes for mixed $1(b)\,^3\Pi_0(v_b,J)\sim 2(A)\,^1\Sigma^+(v_A,J)$ levels near the $1(b)\,^3\Pi_0(v_b=12,J=38)\sim 2(A)\,^1\Sigma^+(v_A=11,J=38)$ center of perturbation recorded using the copropagating laser geometry. J values range from 37 to 40.

$$\cos^2\theta = \frac{(U-E^0_\Sigma)^2}{|H_{\rm SO}|^2+(U-E^0_\Sigma)^2} = \frac{|H_{\rm SO}|^2}{(E^0_\Sigma-L)^2+|H_{\rm SO}|^2} = \frac{\Delta U}{\Delta U+\Delta L} \tag{14}$$

and

$$\sin^2\theta = \frac{\Delta L}{\Delta U+\Delta L}. \tag{15}$$

According to Eq. (13), the denominators in Eqs. (14) and (15) are equal to $E^0_{\Pi i+1}-E^0_{\Pi i}$. With this in mind, we note that these equations show that the mixing probabilities are simply related to the way the unperturbed hyperfine splitting is shared between the upper and lower states of an interacting pair.

IV. RESULTS

Figure 2 shows the measured line shapes for mixed $1(b)^3\Pi_0(v_b,J)\sim 2(A)\,^1\Sigma^+(v_A,J)$ levels near the strong $1(b)\,^3\Pi_0(12,38)\sim 2(A)^1\Sigma^+(11,38)$ perturbation. The selected data illustrate how levels lying near the centers of perturbation contain strong admixtures of both singlet and triplet character, while levels lying further away from the centers of perturbation exhibit mostly unperturbed line shape signatures. The relatively unperturbed $1(b)\,^3\Pi_0$ line shapes away from the center of perturbation clearly exhibit the four peaks predicted by the analysis of Sec. III A.

The analysis presented in Sec. III B considered pairs of hyperfine levels for each of the two interacting states $1(b)^3\Pi_0(v_b,J)$ and $2(A)\,^1\Sigma^+(v_A,J)$. In order to apply this model to the present situation, in which each of the two interacting rovibrational levels has four hyperfine levels, we regard U, ΔU, L, and ΔL as the average energies and hyperfine splittings of the upper and lower perturbed levels, respectively. With our current resolution, we find that hyperfine splittings of less than $\sim 0.002\ \mathrm{cm}^{-1}$ are often too small to resolve directly. However, Fig. 2 shows that even then the observed perturbed level spectral lines are definitely broader than those of a pure singlet level. In all cases, we determined the hyperfine splittings from the measured signals by modeling each line as a sum of four equally spaced Lorentzians and varying their separation to match the overall experimental structure and line widths. The observed splittings of the PFOODR spectral lines, $\Delta E^{\rm obs}_{U,L}$, were then divided by $[1+(\omega_{\rm probe}/\omega_{\rm pump})]_{U,L}$ to obtain the upper and lower $1(b)\,^3\Pi_0 \sim 2(A)\,^1\Sigma^+$ perturbed level hyperfine splittings ΔU and ΔL. According to Eq. (13), the unperturbed $1(b)\,^3\Pi_0$ level hyperfine splittings are just given by the sum of ΔU and ΔL. Values of these quantities are available in Table 1 of the accompanying EPAPS documentation.[53]

The sum of ΔU and ΔL is just the quantity $\Delta E^0_{\rm hfs}$ considered in the analysis of Sec. III A. Therefore, each pair of the mutually perturbing levels provides a value of $\Delta E^0_{\rm hfs}$ for an unperturbed $1(b)^3\Pi_0$ state. The corresponding value of χ [defined by Eq. (4)] can be calculated using the spectroscopic constants B_v and A_v of the $1(b)\,^3\Pi$ state determined by Ross *et al.*[18] The experimental values of $\Delta E^0_{\rm hfs}$ and the best fit curve of the form $\Delta E^0_{\rm hfs}=b_{\rm F}\chi/\sqrt{1+\chi^2}$ are plotted as a function of χ in Fig. 3. The data and fit provide a striking demonstration of the approach to the pure case (a) limit as $\chi\to 0$. Since the ratio B/A only changes a few percent for the

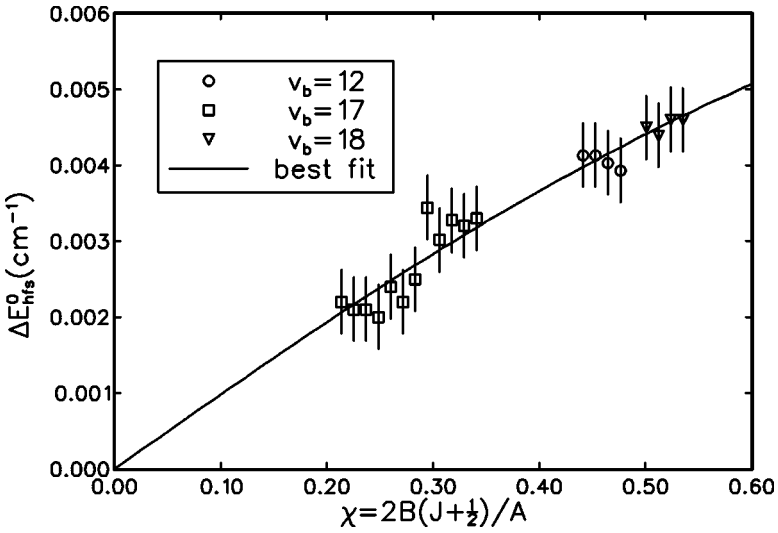

FIG. 3. The sum $\Delta U+\Delta L=\Delta E^0_{\rm hfs}$ of the experimentally measured hyperfine splittings for several mutually perturbing $1(b)\,^3\Pi_0 \sim 2(A)\,^1\Sigma^+$ rovibrational pairs. $\Delta E^0_{\rm hfs}$ corresponds to the splitting that each $1(b)\,^3\Pi_0$ level would have if it were unperturbed by the nearby $2(A)\,^1\Sigma^+$ level. Three groups of points are shown, corresponding to vibrational quantum numbers $v_b=12$, 17, and 18. The error bars ($\pm 0.000\,42$ cm^{-1}) correspond to the statistical uncertainty in the data. The value of χ determines where a particular level lies between Hund's case (a) and case (b). $\chi=0$ corresponds to pure case (a), for which the hyperfine splitting is zero. The curve shows the best fit to the data, obtained for $b_{\rm F}=0.009\,89$ cm^{-1}. The statistical error estimate for $b_{\rm F}$ is about ±3%.

three vibrational levels of the $1(b)\,^3\Pi_0$ state investigated, the change in χ is almost entirely due to the change in J. These results clearly show that the $1(b)\,^3\Pi_0$ state exhibits significant hyperfine structure because it is not pure case (a), and that the magnitude of this structure is strongly dependent on J.

The value reported for the Fermi contact constant $b_{\rm F}$ was determined by noting that a value of $b_{\rm F}$ can be explicitly obtained from each pair of mutually perturbing levels $(\chi, \Delta E^0_{\rm hfs}=\Delta U+\Delta L)$ using Eq. (3), $b_{\rm F}=\Delta E^0_{\rm hfs}\sqrt{1+\chi^2}/\chi$, and the known values of B_v and A_v for the NaK $1(b)\,^3\Pi$ state from Ross *et al.*[18] These $b_{\rm F}$ values are listed in EPAPS Table 1.[53] The best value and its statistical uncertainty can be determined by averaging the values of $b_{\rm F}$ from each data point, with an appropriate weighting factor. For our case, we estimate a statistical uncertainty of 0.0003 cm^{-1} for each of the measured ΔU and ΔL values, leading to a (constant) statistical uncertainty of $[(0.0003)^2+(0.0003)^2]^{1/2}=0.000\,42$ cm^{-1} in $\Delta E^0_{\rm hfs}$, which is the main source of uncertainty in the $b_{\rm F}$ values. The final best-fit value is

$$b_{\rm F}=(0.009\,89\pm 0.000\,27)\ {\rm cm}^{-1}. \tag{16}$$

A least squares fit using the 12×12 spin–orbit/hyperfine matrix diagonalization method gives essentially the same result.

The value of $b_{\rm F}$ we report here is within a few percent of the values measured for the $2(c)\,^3\Sigma^+$, $1\,^3\Delta$, and $4\,^3\Sigma^+$ electronic states of NaK.[11,13,37,38,54,55] [The value reported for the Fermi contact constant of the NaK $4\,^3\Sigma^+$ state in Ref. 13 (page 4752) should read (0.0099 ± 0.0004) cm^{-1} rather than (0.99 ± 0.04) cm^{-1}. The correct value was given in the abstract of that reference.]

Values for the $1(b)\,^3\Pi_0 \sim 2A\,^1\Sigma^+$ spin–orbit matrix element $|H_{\rm SO}|$ were determined from the measured hyperfine splittings for 20 sets of mutually perturbing pairs, using the final form of Eq. (10). Estimates confirmed that the dropped term makes a negligible contribution. The values for $|H_{\rm SO}|$ are listed in EPAPS Table 2.[53] The statistical uncertainties of these values arise in part from the 0.01 cm^{-1} uncertainty of the absolute line positions, but mostly from the 0.0003 cm^{-1} uncertainty of the measured line splittings, ΔU and ΔL.

As discussed in Refs. 24 and 56, the spin–orbit operator acts primarily on the electronic part of the wave functions. Thus by factoring the total wave function into products of electronic, vibrational, and rotational wave functions, we may define a quantity $H_{\rm el}$ that depends primarily on the interacting electronic wave functions,

$$H_{\rm el}\approx \frac{\langle 1(b)\,^3\Pi_0(v_b,J)|\mathbf{H}_{\rm SO}|2(A)^1\Sigma^+(v_A,J)\rangle}{\langle v_b|v_A\rangle}. \tag{17}$$

However, in writing the upper and lower state wave functions as linear combinations of unperturbed $2(A)\,^1\Sigma^+$ and $1(b)\,^3\Pi_0$ wave functions in Eqs. (6) and (7), we neglect the rotational coupling between the $1(b)\,^3\Pi_\Omega$ levels. Instead, each "unperturbed" $1(b)\,^3\Pi_0$ level should be written more correctly as a linear combination $a'|1(b)\,^3\Pi_0(v_b,J)\rangle + b'|1(b)\,^3\Pi_1(v_b,J)\rangle + c'|1(b)\,^3\Pi_2(v_b,J)\rangle$. As explained in Refs. 2 and 24 each spin–orbit matrix element obtained from the data using the two-state analysis must also be divided by the mixing coefficient a' to obtain the underlying $1(b)\,^3\Pi_0 \sim 2(A)\,^1\Sigma^+$ spin–orbit matrix element:

$$H_{\rm el}=\frac{\langle 1(b)^3\Pi_0(v_b,J)|\mathbf{H}_{\rm SO}|2(A)^1\Sigma^+(v_A,J)\rangle}{a'\langle v_b|v_A\rangle}. \tag{18}$$

Using the program LSQ (Ref. 57) we calculated values of a' ranging from 0.942 to 0.989 [see EPAPS Table 3 (Ref. 53)]. The vibrational overlap integrals in the denominator were calculated from the experimental Rydberg–Klein–Rees (RKR) potentials for the $2(A)\,^1\Sigma^+$ and $1(b)\,^3\Pi_0$ states given in Refs. 20 and 18, respectively, using the program LEVEL7.5.[58] Figure 4 and EPAPS Table 3 (Ref. 53) show the values of $|H_{\rm el}|$ for each mutually perturbing pair. Note that the uncertainty in $|H_{\rm el}|$ is much smaller for levels near the centers of perturbation that have comparable singlet and triplet amplitudes. The weighted mean value for $|H_{\rm el}|$ determined using the technique described here is

$$|H_{\rm el}|=(16.33\pm 0.15)\ {\rm cm}^{-1}, \tag{19}$$

where the quoted error bar represents statistical uncertainty only. The systematic error could be as high as 2%–3% if, for example, our method for fitting the data systematically over-

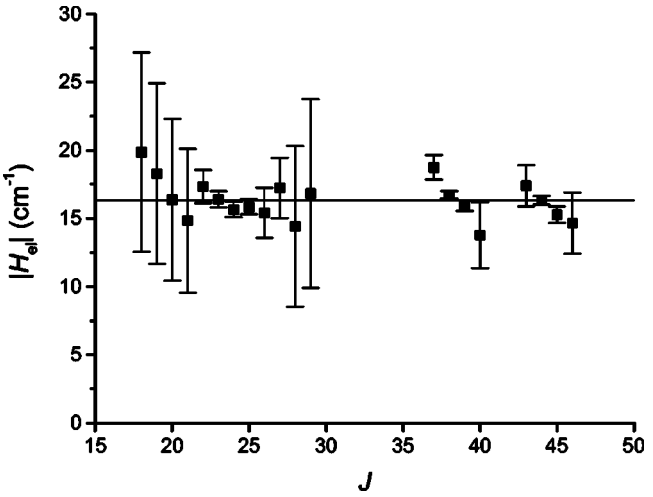

FIG. 4. Values of $|H_{el}|$ determined from measured energies and hyperfine splittings of mutually perturbing NaK $1(b)\,^3\Pi_0(v_b,J) \sim 2(A)\,^1\Sigma^+(v_A,J)$ rovibrational levels. The solid horizontal line represents the weighted average of the results [cf. Eq. (19)].

estimates or underestimates the hyperfine splittings.

Finally, the unperturbed energies E_Σ^0 and E_Π^0 and the mixing probabilities, for each level studied, were determined using Eqs. (11), (12), (14), and (15). These values are also given in EPAPS Table 2.[53] As expected, the mixing coefficients and unperturbed level energies show that the mixing and the magnitudes of the energy shifts $E_\Pi - E_\Pi^0$ and $E_\Sigma - E_\Sigma^0$ are greatest for those $1(b)\,^3\Pi_0(v_b,J)$ and $2(A)\,^1\Sigma^+(v_A,J)$ level pairs that lie closest in energy. For a given $v_b \sim v_A$ manifold, as one moves away from the center of perturbation (by changing rotational quantum number J) the levels are less mixed since the unperturbed level separation is greater.

V. CONCLUSIONS

This work has investigated the electronic coupling between different molecular potential energy curves using high-resolution hyperfine spectroscopy. By measuring the size of the hyperfine splitting in several mixed rovibrational levels of the NaK $1(b)\,^3\Pi_0$ and $2(A)\,^1\Sigma^+$ states, we have been able to infer the strength of the electronic coupling between these two states.

The present value of $|H_{el}|$ for NaK is ~4% higher than our previous value and slightly outside combined error bars. However, the quoted error bars for the present work and in Ref. 24 represent statistical uncertainties only. We believe that the present measurement is more accurate than our previous value,[24] but the main advantage of the present work is that the determination of each spin–orbit matrix element $\langle 1(b)\,^3\Pi_0(v_b,J)|\mathbf{H}_{SO}|2(A)\,^1\Sigma^+(v_A,J)\rangle$ is entirely self-contained and therefore less likely to be affected by systematic error. The current method essentially requires no knowledge of unperturbed level positions that cannot be observed directly.

We also investigated the origin of the hyperfine splitting in the $\Omega=0$ component of the NaK $1(b)\,^3\Pi$ state. Electric quadrupole terms are known to make only very small contributions to the hyperfine structure of alkali molecules, and formulas based on the pure Hund's case (a) limit suggest that the magnetic dipole hyperfine structure of a $^3\Pi_0$ state should be negligible. Our analysis and measurements have provided a quantitative demonstration that significant hyperfine splitting arises in the NaK $1(b)\,^3\Pi_0$ state precisely because the angular momentum coupling is not pure case (a). The magnitude of the hyperfine splitting varies strongly with J, with smaller J corresponding to coupling closer to pure case (a).

Because spectroscopic constants[18] are available for the NaK $1(b)\,^3\Pi_0$ state, we were able to extract an accurate value for the Fermi contact constant for that state from our measurements. The value that best fits the data, $b_F = (0.009\,89 \pm 0.000\,27)$ cm^{-1}, is very similar to the value obtained for other NaK electronic states with similar molecular orbitals. This agreement lends credence to the reliability of our conclusions, but it also raises the possibility that other NaK electronic states with significantly different molecular orbitals (most notably the $3\,^3\Pi$ state)[51] will have different Fermi contact constants. As has been demonstrated, for example by Levenson and Schawlow[59] and Bacis and co-workers[60] for I_2 and by Janda and co-workers[61–64] for ICl, measurements of the hyperfine structure can serve as a very sensitive probe of the molecular electronic wave function. Our ongoing and future work will exploit this relationship to gain a deeper understanding of the electronic states of heteronuclear alkali molecules.

[1] Li Li and R. W. Field, J. Phys. Chem. **87**, 3020 (1983).
[2] X. Xie and R. W. Field, J. Mol. Spectrosc. **117**, 228 (1986).
[3] Li Li, Q. Zhu, and R. W. Field, J. Mol. Spectrosc. **134**, 50 (1989).
[4] Li Li, Q. Zhu, and R. W. Field, Mol. Phys. **66**, 685 (1989).
[5] Li Li, T. An, T.-J. Whang, A. M. Lyyra, W. C. Stwalley, R. W. Field, and R. A. Bernheim, J. Chem. Phys. **96**, 3342 (1992).
[6] A. Yiannopoulou, K. Urbanski, A. M. Lyyra, Li Li, B. Ji, J. T. Bahns, and W. C. Stwalley, J. Chem. Phys. **102**, 3024 (1995).
[7] J. T. Kim, H. Wang, C. C. Tsai, J. T. Bahns, W. C. Stwalley, G. Jong, and A. M. Lyyra, J. Chem. Phys. **102**, 6646 (1995); **103**, 9891(E) (1995).
[8] Li Li, A. Yiannopoulou, K. Urbanski, A. M. Lyyra, B. Ji, W. C. Stwalley, and T. An, J. Chem. Phys. **105**, 6192 (1996); **106**, 8626(E) (1997).
[9] G. Lazarov, A. M. Lyyra, Li Li, and J. Huennekens, J. Mol. Spectrosc. **196**, 259 (1999).
[10] Li Li and A. M. Lyyra, Spectrochim. Acta, Part A **55**, 2147 (1999).
[11] J. Huennekens, I. Prodan, A. Marks, L. Sibbach, E. Galle, T. Morgus, and Li Li, J. Chem. Phys. **113**, 7384 (2000).
[12] Y. Liu, B. Ji, A. S.-C. Cheung, W. C. Stwalley, R. W. Field, A. M. Lyyra, and Li Li, J. Chem. Phys. **115**, 3647 (2001).
[13] P. Burns, L. Sibbach-Morgus, A. D. Wilkins, F. Halpern, L. Clarke, R. D. Miles, Li Li, A. P. Hickman, and J. Huennekens, J. Chem. Phys. **119**, 4743 (2003).
[14] P. Yi, X. Dai, J. Li, Y. Liu, Li Li, V. B. Sovkov, and V. S. Ivanov, J. Mol. Spectrosc. **225**, 33 (2004).
[15] X. Xie and R. W. Field, Chem. Phys. **99**, 337 (1985).
[16] C. Effantin, O. Babaky, K. Hussein, J. d'Incan, and R. F. Barrow, J. Phys. B **18**, 4077 (1985).
[17] O. C. Mullins, C. R. Mahon, and T. F. Gallagher, Chem. Phys. Lett. **126**, 501 (1986).
[18] A. J. Ross, C. Effantin, J. d'Incan, and R. F. Barrow, J. Phys. B **19**, 1449 (1986).
[19] A. J. Ross, P. Crozet, C. Effantin, J. d'Incan, and R. F. Barrow, J. Phys. B **20**, 6225 (1987).
[20] A. J. Ross, R. M. Clements, and R. F. Barrow, J. Mol. Spectrosc. **127**, 546 (1988).
[21] H. Katô, M. Otani, and M. Baba, J. Chem. Phys. **89**, 653 (1988).
[22] O. Babaky and K. Hussein, Z. Naturforsch., A: Phys. Sci. **45**, 795 (1990).
[23] T.-J. Whang, W. C. Stwalley, Li Li, and A. M. Lyyra, J. Chem. Phys. **97**, 7211 (1992).
[24] H. Sun and J. Huennekens, J. Chem. Phys. **97**, 4714 (1992).

[25]A. V. Stolyarov, I. P. Klincare, M. Ya. Tamanis, and R. S. Ferber, J. Chem. Phys. **98**, 826 (1993).
[26]L. M. Andersson, H. O. Karlsson, O. Goscinski, L.-E. Berg, M. Beutter, and T. Hansson, Chem. Phys. **241**, 43 (1999).
[27]R. Ferber, E. A. Pazyuk, A. V. Stolyarov, A. Zaitsevskii, P. Kowalczyk, H. Chen, H. Wang, and W. C. Stwalley, J. Chem. Phys. **112**, 5740 (2000).
[28]M. R. Manaa, A. J. Ross, F. Martin, P. Crozet, A. M. Lyrra, Li Li, C. Amiot, and T. Bergeman, J. Chem. Phys. **117**, 11208 (2002).
[29]M. Tamanis, R. Ferber, A. Zaitsevskii, E. A. Pazyuk, A. V. Stolyarov, H. Chen, J. Qi, H. Wang, and W. C. Stwalley, J. Chem. Phys. **117**, 7980 (2002).
[30]T. Bergeman, C. E. Fellows, R. F. Gutterres, and C. Amiot, Phys. Rev. A **67**, 050501(R) (2003).
[31]A. Gallagher and D. E. Pritchard, Phys. Rev. Lett. **63**, 957 (1989).
[32]P. S. Julienne and J. Vigué, Phys. Rev. A **44**, 4464 (1991).
[33]W. Preuss and G. Baumgartner, Z. Phys. A **320**, 125 (1985).
[34]G. Baumgartner, H. Kornmeier, and W. Preuss, Chem. Phys. Lett. **107**, 13 (1984).
[35]J. B. Atkinson, J. Becker, and W. Demtröder, Chem. Phys. Lett. **87**, 128 (1982).
[36]C. Lisdat, H. Knöckel, and E. Tiemann, J. Mol. Spectrosc. **199**, 81 (2000).
[37]K. Ishikawa, T. Kumauchi, M. Baba, and H. Katô, J. Chem. Phys. **96**, 6423 (1992).
[38]P. Kowalczyk, J. Chem. Phys. **91**, 2779 (1989).
[39]R. A. Frosch and H. M. Foley, Phys. Rev. **88**, 1337 (1952).
[40]C. H. Townes and A. L. Schawlow, *Microwave Spectroscopy* (McGraw-Hill, New York, 1955).
[41]H. Katô, Bull. Chem. Soc. Jpn. **66**, 3203 (1993).
[42]K. Ishikawa, J. Chem. Phys. **98**, 1916 (1993).
[43]C. R. Vidal and J. Cooper, J. Appl. Phys. **40**, 3370 (1969).
[44]S. Gerstenkorn and P. Luc, *Atlas du Spectre D'Absorption de la Molécule D'Iode* (Centre National de la Recherche Scientifique, Paris, 1978).
[45]I. Kovács, *Rotational Structure in the Spectra of Diatomic Molecules* (American Elsevier, New York, 1969).
[46]J. M. Brown, E. A. Colbourn, J. K. G. Watson, and F. D. Wayne, J. Mol. Spectrosc. **74**, 294 (1979).
[47]R. N. Zare, A. L. Schmeltekopf, W. J. Harrop, and D. L. Albritton, J. Mol. Spectrosc. **46**, 37 (1973).
[48]R. N. Zare, *Angular Momentum* (Wiley, New York, 1988).
[49]D. L. Huestis, in *Atomic, Molecular, and Optical Physics Handbook*, edited by G. W. F. Drake (AIP, Woodbury, NY, 1996).
[50]W. J. Stevens, D. D. Konowalow, and L. B. Ratcliff, J. Chem. Phys. **80**, 1215 (1984).
[51]R. D. Miles, A. D. Wilkens, L. Morgus, J. Huennekens, and A. P. Hickman (unpublished).
[52]P. Burns, Ph.D. dissertation, Lehigh University, 2004.
[53]See EPAPS Document No. E-JCPSA6-122-004505, for three tables of related information. A direct link to this document may be found in the online article's HTML reference section. The document may also be reached via the EPAPS homepage (http://www.aip.org/pubservs/epaps.html) or from ftp.aip.org in the directory /epaps/. See the EPAPS homepage for more information.
[54]P. Kowalczyk, B. Krüger, and F. Engelke, Chem. Phys. Lett. **147**, 301 (1988).
[55]M. Baba, K. Nishizawa, N. Yoshie, K. Ishikawa, and H. Katô, J. Chem. Phys. **96**, 955 (1992).
[56]H. Lefebvre-Brion and R. W. Field, *Perturbations in the Spectra of Diatomic Molecules* (Academic, Orlando, FL, 1986).
[57]R. A. Gottscho, J. B. Koffend, and R. W. Field, J. Mol. Spectrosc. **82**, 310 (1980).
[58]R. J. Leroy, "LEVEL7.5: A Computer Program for Solving the Radial Schrödinger Equation for Bound and Quasibound Levels," Chemical Physics Research Report No. CP-655, University of Waterloo, 2002.
[59]M. D. Levenson and A. L. Schawlow, Phys. Rev. A **6**, 10 (1972).
[60]R. Bacis, M. Broyer, S. Churassy, J. Vergès, and J. Vigué, J. Chem. Phys. **73**, 2641 (1980).
[61]C. M. Western, T. J. Slotterback, J. R. Johnson, D. W. Pratt, and K. C. Janda, J. Chem. Phys. **98**, 1826 (1993).
[62]T. J. Slotterback, S. G. Clement, K. C. Janda, and C. M. Western, J. Chem. Phys. **101**, 7221 (1994).
[63]C. M. Western, W. S. Barney, S. G. Clement, T. J. Slotterback, and K. C. Janda, Z. Phys. D: At., Mol. Clusters **36**, 273 (1996).
[64]W. S. Barney, C. M. Western, and K. C. Janda, J. Chem. Phys. **113**, 7211 (2000).